Published October 31, 2011

Follicular dendritic cells help establish follicle identity and promote B cell retention in germinal centers

Xiaoming Wang,[1,2] Bryan Cho,[1,2] Kazuhiro Suzuki,[1,2] Ying Xu,[1,2] Jesse A. Green,[1,2] Jinping An,[1,2] and Jason G. Cyster[1,2]

[1]Howard Hughes Medical Institute and [2]Department of Microbiology and Immunology, University of California, San Francisco, San Francisco, CA 94143

Follicular dendritic cells (FDCs) retain and display opsonized antigens in primary follicles and germinal centers (GCs). However, their roles beyond antigen presentation have been incompletely defined. In this study, we tested the impact of selective FDC ablation on short-term follicle and GC function. Within 2 d of FDC ablation, primary follicles lost their homogeneity and became disorganized bands of cells around T zones. These B cell areas retained CXCL13-expressing stromal cells but often exhibited inappropriate ER-TR7 and CCL21 expression. Ablation of GC FDCs led to the disappearance of GCs. When B cell death was prevented using a Bcl2 transgene, FDC ablation led to splenic GC B cell dispersal. Mesenteric lymph node GCs were more resistant but became dispersed when sphingosine-1-phosphate receptor-2 was also removed. These experiments indicate that FDCs help maintain primary follicles as a B cell exclusive niche and define a critical role for FDCs in cell retention within GCs.

CORRESPONDENCE
Jason G. Cyster:
Jason.Cyster@ucsf.edu

Abbreviations used: DP, double positive; DTR, DTx receptor; DTx, diphtheria toxin; FDC, follicular DC; GC, germinal center; mLN, mesenteric LN; mRNA, messenger RNA; pLN, peripheral LN; SRBC, sheep RBC.

Early antigen-tracing experiments established that cells within the center of follicles captured and retained opsonized antigens for long periods. Ultrastructural studies led to the description of a highly dendritic-shaped cell that was responsible for antigen capture and display, and these cells became known as follicular DCs (FDCs; Szakal et al., 1989; Tew et al., 1993). FDCs within primary follicles express high amounts of complement receptors-1 and -2 (CR1 or CD35 and CR2 or CD21) and can be induced to express FcγRIIb (Roozendaal and Carroll, 2007; Allen and Cyster, 2008). FDCs are also prominent in the light zone of germinal centers (GCs), where they express FDC-M1 (MFG-E8) and VCAM-1, and are heavily decorated with activated C4 (Allen and Cyster, 2008; Kranich et al., 2008). The stromal cells around the follicle perimeter express some markers in common with FDCs, such as BP3 (CD157), but are otherwise distinct from FDCs and from ER-TR7–expressing T zone stromal cells (Cyster et al., 2000). The stromal cells in the outer follicle have been classified as marginal reticular cells (Katakai et al., 2008).

FDCs develop within follicles after the arrival of B cells (Balogh et al., 2001), and their induction is dependent on LTα1β2 derived from B cells, as well as TNF from B cells and additional cell types (Fu and Chaplin, 1999; Allen and Cyster, 2008). Although their developmental pathway has not been fully elucidated, they are radiation resistant and are considered to be mesenchymal in origin (Tew et al., 1993; Cyster et al., 2000; Allen and Cyster, 2008). B cell recruitment to nascent follicles is dependent on CXCL13, the chemokine ligand for CXCR5 (Cyster et al., 2000). CXCL13 is expressed early in lymphoid tissue development, and expression is augmented by LTα1β2 (Cupedo et al., 2004; Allen and Cyster, 2008). CXCL13 is made in a reticular pattern that overlaps with both the non-FDC and FDC stromal networks (Cyster et al., 2000). However, the relative contribution of non-FDC stromal cells and FDCs to CXCL13 production has not been defined.

The antigen presentation role of FDCs has been supported by in vivo and in vitro studies

The Rockefeller University Press $30.00
J. Exp. Med. Vol. 208 No. 12 2497-2510
www.jem.org/cgi/doi/10.1084/jem.20111449

Published October 31, 2011

(Victoratos et al., 2006; Roozendaal and Carroll, 2007; Suzuki et al., 2009; El Shikh et al., 2010). Additional functions for the cells, such as serving as a source of BAFF (Hase et al., 2004; Suzuki et al., 2010) and promoting GC B cell mutation (El Shikh et al., 2010), have been suggested, but these roles have not been rigorously tested in vivo. Experiments in lymphotoxin- and TNF-deficient mice have provided important correlations regarding a requirement for FDCs in the organization of primary follicles and in mounting GC responses (Fu and Chaplin, 1999; Allen and Cyster, 2008). However, inferences about the roles of FDCs made through these studies are confounded by the fact that these cytokines are needed for multiple functions, including chemokine and integrin ligand expression by the entire lymphoid stroma (Ngo et al., 1999; Lu and Cyster, 2002; Browning, 2008) and for the maintenance of various lymphoid tissue macrophages and DCs (Kabashima et al., 2005; Wang et al., 2005; Browning, 2008; Phan et al., 2009). Selective genetic restoration of TNFR1 within FDCs in mice that otherwise lacked this receptor provided more direct evidence that FDCs are required for follicle development and efficient GC formation (Victoratos et al., 2006). In these animals, FDCs were restored from early development and thus their role in maintaining the follicle or in supporting established GC responses was not assessed.

In this study, we have used a short-term conditional ablation system to study the role of FDCs in primary follicles and GCs. We show that FDC ablation before immunization leads to a rapid disruption in follicular organization and a reduction in B cell motility. Ablation of FDCs during the GC response causes rapid GC B cell dispersal and death. These observations suggest that FDCs help establish primary follicle identity, and they act to retain and promote the survival of GC B cells.

RESULTS

FDC ablation in CD21-Cre × ROSA^{DTR} mice

CD21 expression in the immune system is restricted to FDCs and B cells (Roozendaal and Carroll, 2007), and in CD21-Cre mice, Cre is highly active in these cells types (Victoratos et al., 2006). With the goal of generating mice that allowed selective diphtheria toxin (DTx)–mediated ablation of FDCs, CD21-Cre mice were intercrossed with mice harboring the DTx receptor (DTR) gene downstream of a floxed stop element in the ubiquitously active ROSA26 locus (ROSA^{DTR} mice). Cells in these mice expressing CD21 also express DTR and are selectively vulnerable to deletion on exposure to DTx. The resulting CD21-Cre^{+}ROSA^{DTR+} mice were irradiated and reconstituted with wild-type BM. In these mice (termed CD21-DTR chimeric mice for simplicity), radiation-resistant FDCs were expected to remain sensitive to DTx, whereas B cells would be DTR-negative donor-derived cells and thus toxin resistant. Indeed, when such mice were treated with 20–30 ng DTx (~1 ng/g), amounts similar to or lower than those used in other DTR-based cell deletion experiments, there was ablation of FDCs in spleen, peripheral LNs (pLNs), and mesenteric LNs (mLNs) within 1 d without loss of naive B cells (Fig. 1 A and not depicted). However, the mice showed signs of paralysis and ill health and had elevated circulating corticosteroids within 1–2 d of treatment (Fig. 1 B), requiring their euthanasia. CD21-Cre activity has been detected in brain and kidney (Schmidt-Supprian and Rajewsky, 2007), and we confirmed that DTR transcripts were expressed in these sites (not depicted). We considered the possibility that the toxic effects in CD21-DTR chimeric mice were caused by DTx access to DTR in the brain and speculated that toxin movement across the blood brain barrier might be slow compared with access to FDCs in lymphoid tissues. We therefore tested the protective effect of following DTx treatment after 3 h with injection of DTx-neutralizing polyclonal antibodies. Using this approach, it was possible to achieve ablation of FDCs in spleen and LNs (Fig. 1 A) while maintaining low circulating corticosteroid levels (Fig. 1 B) and normal health during the 2 d of analysis, although longer treatment periods were not possible as the health of the mice deteriorated after day 2. Repeated treatment with DTx-neutralizing antibodies did not allow us to extend the period of study. Treatment of control mice with the same DTx and antibody combination for 2–3 d had no effect on FDCs or mouse health (Fig. 1 A). The 2-d FDC ablation protocol did not alter total cell numbers or B cell frequencies in spleen or LNs (Fig. 1, C and D) or B cell activation status (Fig. 1 E), and there was no change in the rate of B cell, T cell, or CD11c^{+} cell turnover as assessed by bromodeoxyuridine incorporation over the 2 d (not depicted). In all of the experiments described below, DTx treatment was followed at 2.5–3 h by anti-DTx treatment.

FDCs help establish primary follicle identity

Although FDCs are well defined as a major stromal cell type within the central region of the primary follicle, their relationship to the broad follicular stromal network identified by BP3 (McNagny et al., 1991) and CXCL13 (Cyster et al., 2000) has been unclear. In the spleen, FDC ablation left the BP3^{+} follicular stromal cell network largely intact (Fig. 2 A). In contrast, in pLNs, FDC ablation led to a marked depletion of the BP3-expressing follicular stromal cell network (Fig. 2 A). mLNs were more difficult to study in this context because of the constitutive presence of GCs, but from a limited assessment, there was a similar loss of primary follicle BP3 staining as in pLNs (not depicted). These observations reveal a previously unappreciated dichotomy in the stromal organization of spleen and LN follicles and suggest the presence of a greater density of BP3^{+} non-FDC stromal cells in splenic compared with LN follicles. In situ hybridization was used to identify the stromal cells expressing CXCL13. FDC ablation led to a contraction of the area occupied by CXCL13^{+} cells in the spleen, with the strongest remaining signal being at the outer follicle (Fig. 2 B), and there was a corresponding approximately twofold reduction in the CXCL13 transcript abundance in total spleen tissue (Fig. 2 C). In agreement with the overlap in distribution of CXCL13^{+} and CD35^{+} cell distribution, combined CXCL13 in situ hybridization and staining for CD35 in control spleen provided evidence for the presence

Published October 31, 2011

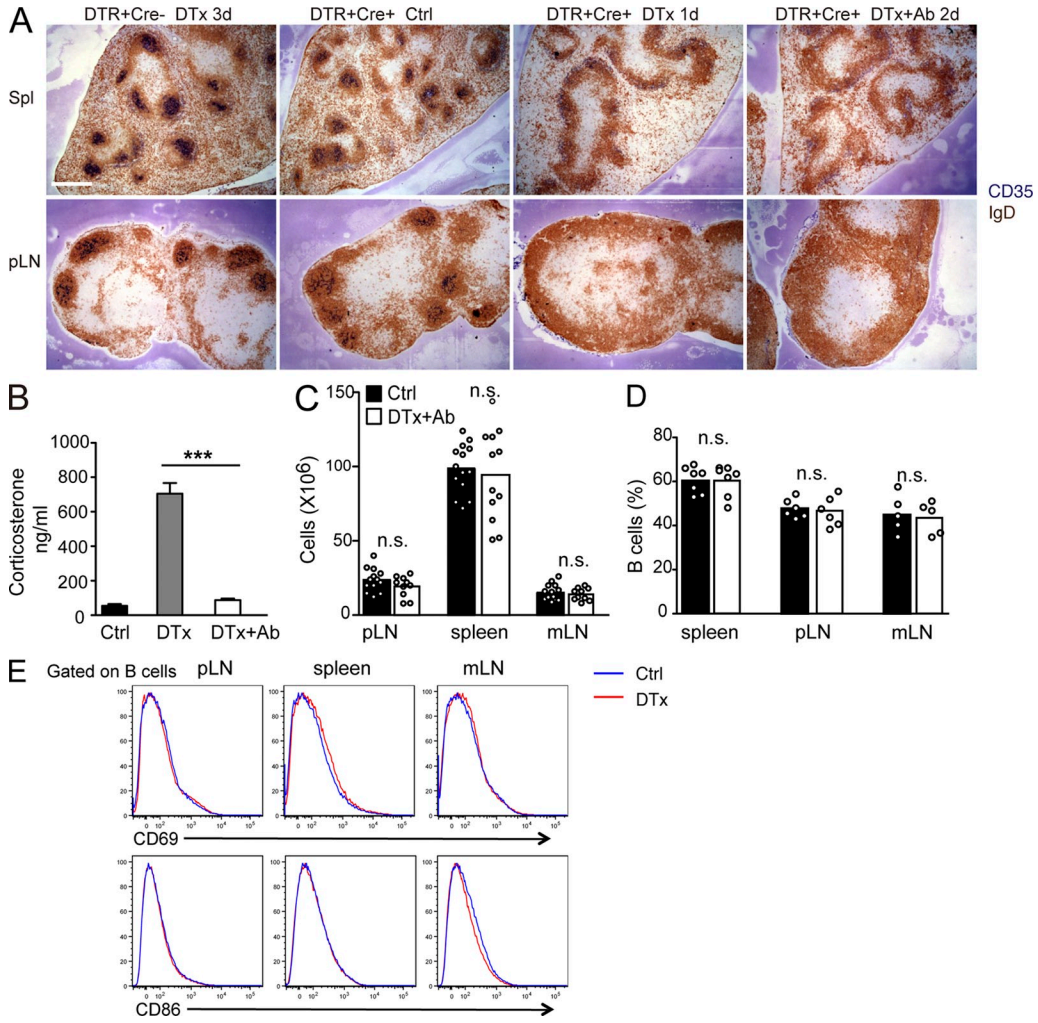

Figure 1. FDC ablation in CD21–DTR chimeric mice after serial DTx and anti–DTx treatment. (A) ROSA^{DTR+}CD21Cre^{+} mice that express the DTR in CD21^{+} cells or ROSA^{DTR+}CD21Cre^{-} control mice were reconstituted with wild-type BM, and the chimeric mice were saline (control [Ctrl]) or DTx treated and analyzed after the indicated number of days. In some cases, the mice were also treated with goat polyclonal antibody to DTx 3 h after DTx treatment (+Ab). Spleen (Spl) and pLN sections were stained for IgD to detect follicular B cells (brown) and CD35 to detect FDCs (blue). Bar, 400 µm. (B) Serum corticosterone concentration in control-, DTx-, or DTx- and anti-DTx antibody–treated CD21-DTR chimeric mice at day 2. Data are pooled from at least eight mice per group analyzed in two experiments (mean ± SEM). (C–E) Total cell number (C), B220^{+} B cell frequency (D), and flow cytometric analysis (E) of B cell CD69 and CD86 expression in pLNs, spleen, and mLNs at day 2 after control or DTx plus anti-DTx antibody treatment. In the bar graphs, each point indicates an individual animal, and bars indicate the mean. Data in E are representative of three mice. Statistical analysis in B–D was performed with a two-tailed unpaired Student's *t* test. ***, $P < 0.001$; n.s., not significant.

of costaining cells (Fig. 2 B). CXCL13 protein distribution in the spleen mirrored the messenger RNA (mRNA) distribution (Fig. 2 D). In pLNs, there was a similar contraction of CXCL13 mRNA and protein distribution after FDC ablation (Fig. 2, B and D), although there was not a measurable change in total transcript abundance (Fig. 2 C). Given that costaining suggested significant colocalization of CXCL13 message and CD35 protein, the lack of reduction in pLN CXCL13 transcripts was surprising but might be a consequence of a compensatory up-regulation by stromal cells in the subcapsular region (Fig. 2 B). In mLNs, FDC ablation led to a similar reduction in CXCL13 mRNA abundance to that observed in the spleen (Fig. 2 C).

Although B cells express CD35, the more abundant expression in FDCs led us to quantitate CD35 transcript levels in whole tissue as a further method for assessing FDC ablation. 2 d after DTx treatment of CD21-DTR chimeric mice, there was a significant reduction in CD35 (*Cr1*) transcripts in total LN samples (Fig. 2 C). The reduction in spleen was less significant, likely because of the B cell preponderance in spleen and the high expression of CD35 by marginal zone B cells (Martin and Kearney, 2002). MFG-E8, recognized by the FDC-M1 antibody, is made by radiation-resistant stromal cells and is detected on the surface of FDCs, at low levels in primary follicles and more abundantly on GC FDCs (Allen and Cyster, 2008; Kranich et al., 2008). Total transcript analysis

Published October 31, 2011

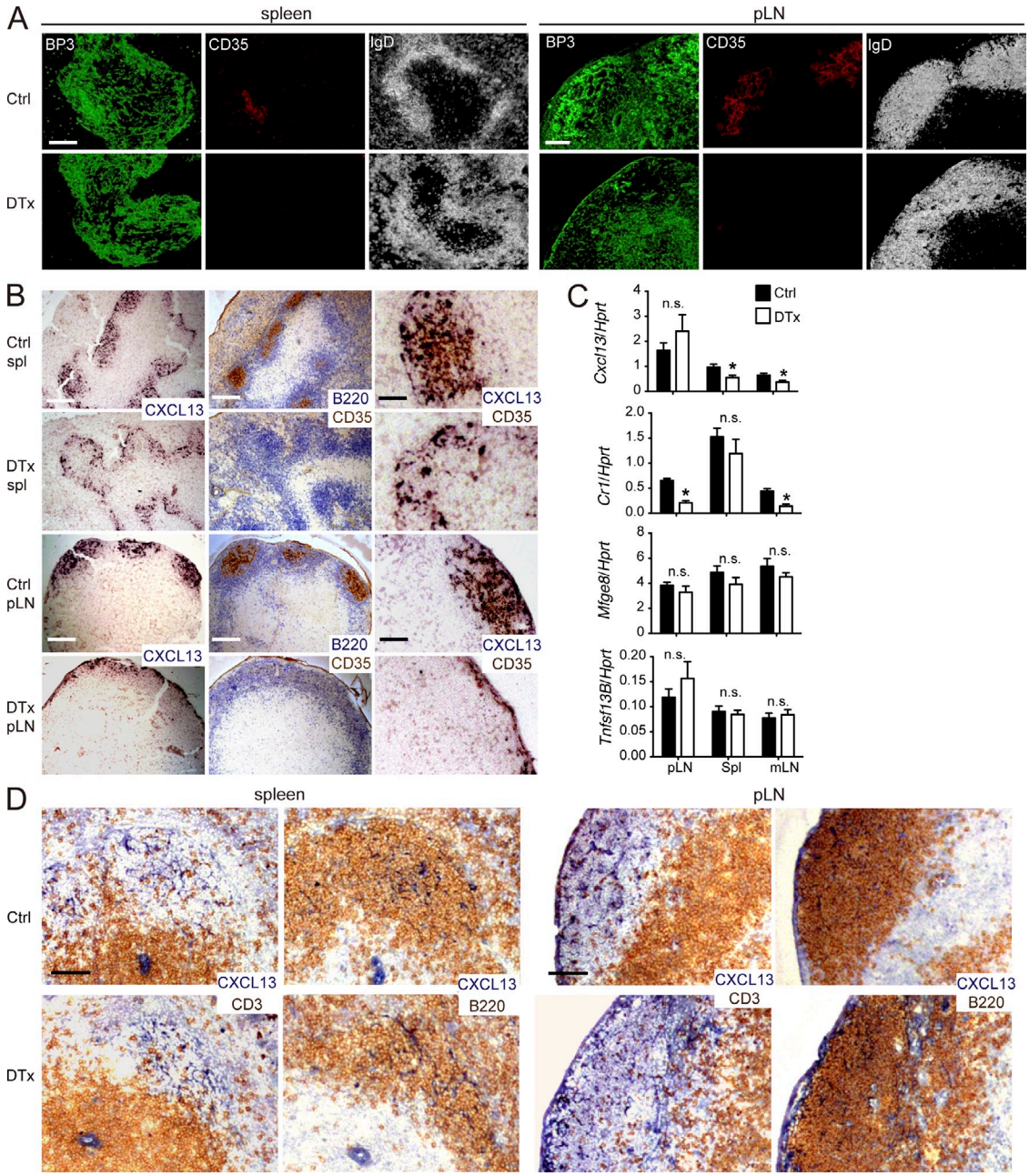

Figure 2. DTx-mediated selective FDC ablation disrupts B cell follicle architecture despite retention of CXCL13. Unimmunized CD21-DTR chimeras were control (Ctrl) or DTx treated 2 d before analysis of spleen (spl) and pLN sections. (A) Immunofluorescence analysis for BP3$^+$ stromal cells, CD35$^+$ FDCs, and IgD$^+$ follicular B cells. (B) In situ hybridization for *Cxcl13* mRNA with serial sections stained for B220 and CD35 or for *Cxcl13* and CD35. (C) Quantitative RT-PCR analysis for *Cxcl13*, *Cr1* (CD35), *Mfge8*, and *Tnsf13B* (BAFF) mRNA in pLNs, spleen, and mLNs, normalized to *Hprt* mRNA. Data are representative of four experiments (mean ± SEM). Statistical analysis was performed with the two-tailed unpaired Student's *t* test. *, $P < 0.05$; n.s., not significant. (D) Immunohistochemical analysis for CXCL13 and CD3 or B220 in serial sections of spleen and pLNs. Data in A, B, and D are representative of at least three experiments (at least two mice of each type per experiment). Bars: (A [left] and B [left and middle]) 200 µm; (A and D, right) 100 µm; (B [right] and D [left]) 50 µm.

revealed only a slight trend for reduced MFG-E8 expression after primary follicle FDC ablation (Fig. 2 C). This result extends previous in situ hybridization data indicating that MFG-E8 is produced broadly by follicular stromal cells (Kranich et al., 2008) and indicates that FDCs may be unique in their ability to capture and display MFG-E8 protein rather than in its expression.

Radiation-resistant stromal cells are an important source of the B cell trophic factor BAFF (Gorelik et al., 2003), and FDCs have been suggested to contribute to this source (Allen and

Published October 31, 2011

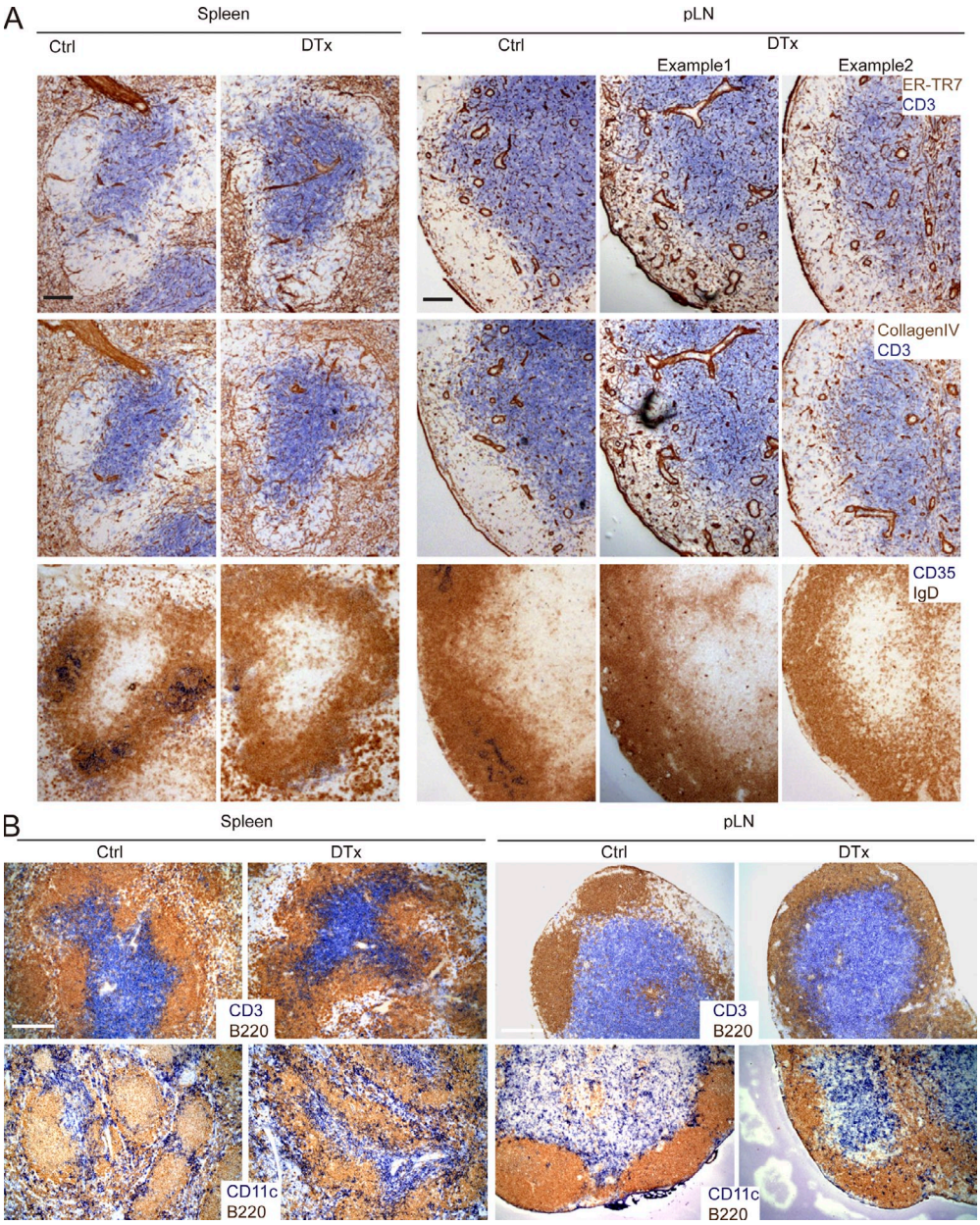

Figure 3. FDC ablation leads to abnormal expression of T zone markers and less restricted positioning of T cells and DCs. Unimmunized CD21-DTR chimeras were control (Ctrl) or DTx treated for 2 d, and spleen and pLN sections were analyzed immunohistochemically as follows. (A) Serial sections were stained for T zone stromal marker ER-TR7 and collagen type IV or for naive B cells with IgD (brown). T cells and FDCs were detected with CD3 and CD35 (blue), respectively. (B) Sections were stained for CD3 to detect T cells (blue), CD11c to detect DCs (blue), and B220 to detect B cells (brown). All data are representative of at least three experiments (at least two mice per experiment). Bars: (A) 100 µm; (B) 200 µm.

Cyster, 2008). However, FDC ablation had no measurable impact on BAFF (*Tnfsf13B*) mRNA levels in total tissue samples (Fig. 2 C), and consistent with this observation, spleen and LN B cell numbers were normal in 2-d FDC-ablated mice (Fig. 1 D).

To further define the properties of the stromal cells present within follicles after FDC ablation, we examined the distribution of the T zone reticular marker, ER-TR7, and collagen type IV. In wild-type follicles, both of these markers were sparsely distributed (Fig. 3 A). However, within 2 d of FDC ablation, there was an increase in the density of both markers in the areas that corresponded to the B cell–rich zones (Fig. 3 A). This increase was typically more evident in the spleen, where the location of the original follicles could be most readily discerned (Fig. 3 A). In LNs, the effect was more variable, with some B cell–rich areas showing little change in the density of these markers and others showing a prominent change (Fig. 3 A). Moreover, T cells and DCs were no longer tightly restricted to the T zone but were now frequently found scattered in considerable numbers

Published October 31, 2011

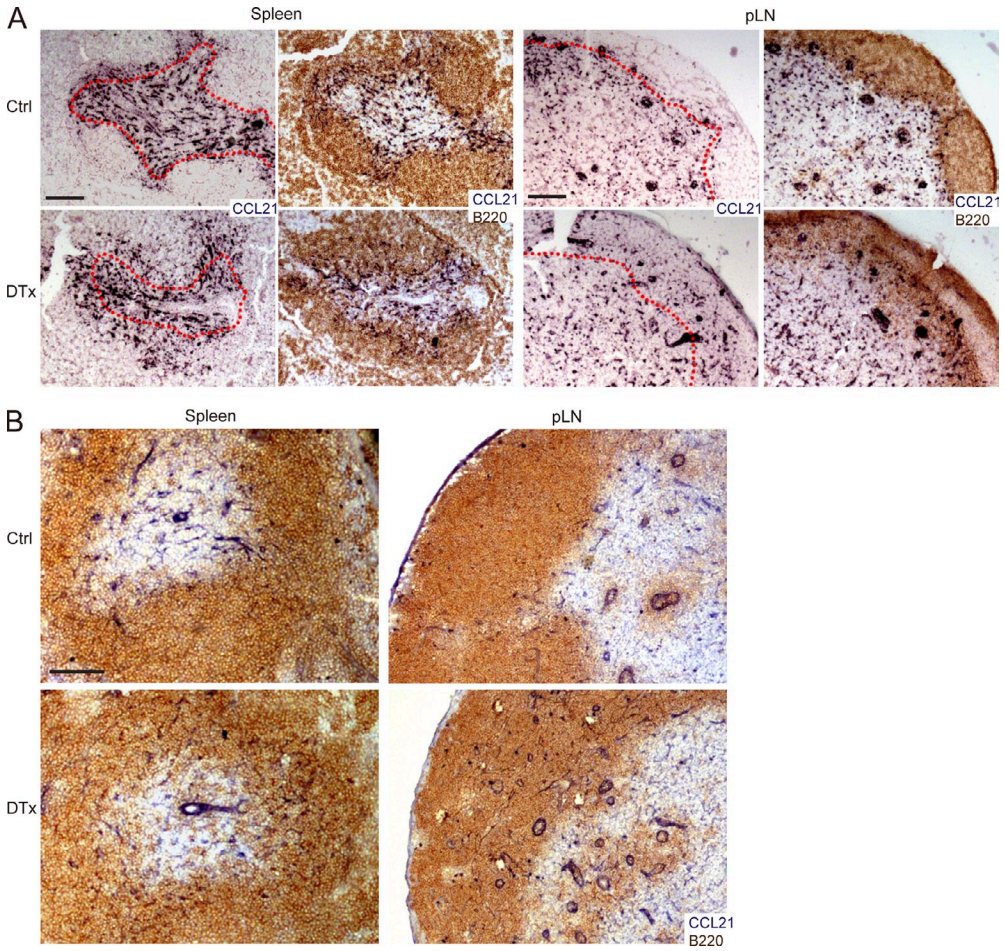

Figure 4. FDC ablation leads to overlap between B cell–rich areas and CCL21-expressing cells. Unimmunized CD21-DTR chimeras were control (Ctrl) or DTx treated for 2 d, and spleen and pLN sections analyzed. (A) In situ hybridization for Ccl21 mRNA (dark blue), detected alone or in combination with staining for B cells (B220; brown). Red dotted lines trace the interface between B cell– and T cell–rich areas, determined based on the adjacent section. (B) Immunohistochemical analysis of CCL21 and B220 in spleen and pLN. Data are representative of at least three mice of each type analyzed in two independent experiments. Bars: (A) 200 µm; (B) 100 µm.

across the boundary into B cell areas of spleen and LNs (Fig. 3 B).

CCL21 mRNA, encoding a chemokine normally restricted to T zone stroma, also now often extended in expression into the B cell–rich areas of spleen and LNs (Fig. 4 A). CCL21 protein was also distributed within B cell areas (Fig. 4 B). This overlap in CCL21 expression likely contributes to the diminished segregation of T cells and DCs from the B cell areas. In contrast, MAdCAM1 expression in the marginal sinus region of spleen remained intact, and $CD169^+$ marginal metallophilic macrophages remained concentrated at the follicle boundary (not depicted).

Altered B cell migration behavior

Previous work has suggested an important role for stromal cells as guides for migrating lymphocytes (Bajénoff et al., 2006). To test whether FDC ablation affected follicular B cell migration, CFSE-labeled B cells and CMTMR-labeled T cells were cotransferred to control and CD21-DTR chimeric mice that were then DTx treated, and cell migration within inguinal LNs was examined 2 d later by two-photon laser scanning microscopy. B cells continued to migrate extensively within the B cell–rich regions of FDC-ablated LNs (Fig. 5 A and Videos 1–4), although their migration velocities were reduced (Fig. 5 B). More strikingly, the cells showed a notable increase in the sharpness of their turning angles (Fig. 5 C). The outcome of this combined reduction in velocity and increase in mean turning angle was an overall reduction in displacement over time (Fig. 5 D). Consistent with the static images, T cells were frequently seen to penetrate deeply into the B cell–rich areas after FDC ablation (Videos 1–4). The relatively modest effect of FDC ablation on naive B cell migration within the B cell–rich areas in pLNs might reflect the continued presence of a stromal cell network in these zones. However, the sharper turning angles of the cells could indicate less effective guidance by this network, with cells detaching more frequently, or a greater amount of stromal cell–independent motility.

Published October 31, 2011

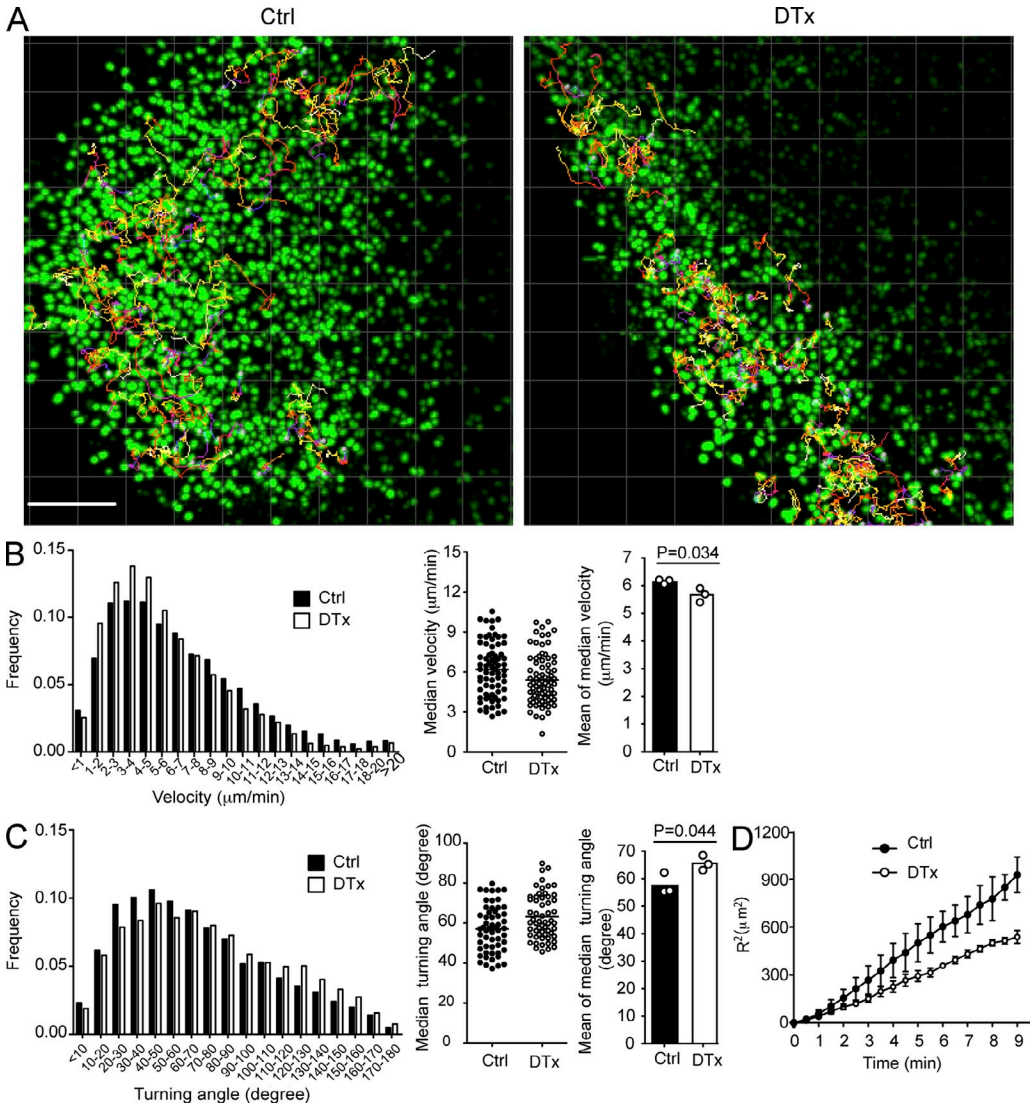

Figure 5. Altered B cell motility in FDC-ablated pLNs. Two-photon laser-scanning microscopy of explanted pLNs from CD21-DTR chimeras that were injected with CFSE-labeled B cells and CMTMR-labeled T cells 5 d before imaging and control (Ctrl) or DTx treated 2 d before imaging. (A) 114-µm maximum intensity z-projection view from a video of control- and DTx-treated LNs, showing the location of CFSE-labeled B cells at a single time point together with measured trajectories of ∼50 B cells. This image corresponds to Videos 1 and 3. Bar, 100 µm. (B and C, left) Instantaneous velocities (B) and turning angles (C) of B cells in pLNs. Central dot plots show medians for each cell track from one representative experiment. Right bar graphs show the mean of the medians from three independent experiments, bars represent means, and circles represent individual experiments. (D) Mean of displacement squared $<R^2>$ over time. Symbols represent means, and error bars represent SEM. Data are representative of three experiments with at least 50 tracks in each. Statistical analysis was performed with the two-tailed unpaired Student's *t* test.

FDC ablation causes acute GC loss

To test the dependence of GCs on FDCs, CD21-DTR chimeric mice were immunized with sheep RBCs (SRBCs) and then treated with DTx at days 6–8, when GCs had formed, and analyzed 2 d later. Flow cytometric analysis revealed a marked (six- to sevenfold) loss of $IgD^{lo}Fas^{hi}GL7^{hi}$ GC B cells from responding pLNs and spleen (Fig. 6 A). The magnitude of the endogenous GC B cell response occurring within the mLNs was similarly affected (Fig. 6 A). Immunohistochemical staining of sections from spleen and LNs showed a very similar picture, with large $GL7^+$ GCs containing well developed $CD35^{hi}$ FDC networks in control mice and a near complete ablation of the GC FDC networks and $GL7^+$ cell clusters in the treated mice (Fig. 6 B and not depicted). An exception was the continued presence of some small FDC-deficient ($CD35^-$) $GL7^+$ B cell clusters in mLNs and occasionally in pLNs (Fig. 6 B). The completeness of GC FDC ablation was further confirmed by the loss of FDC-$M1^+$ and $Fc\gamma RIIb^+$ staining cells (Fig. 6 C). Occasionally, however, there were a few residual FDCs persisting in the treated mice, and these would remain associated with small $GL7^+$ B cell clusters (not depicted). There was also a

Published October 31, 2011

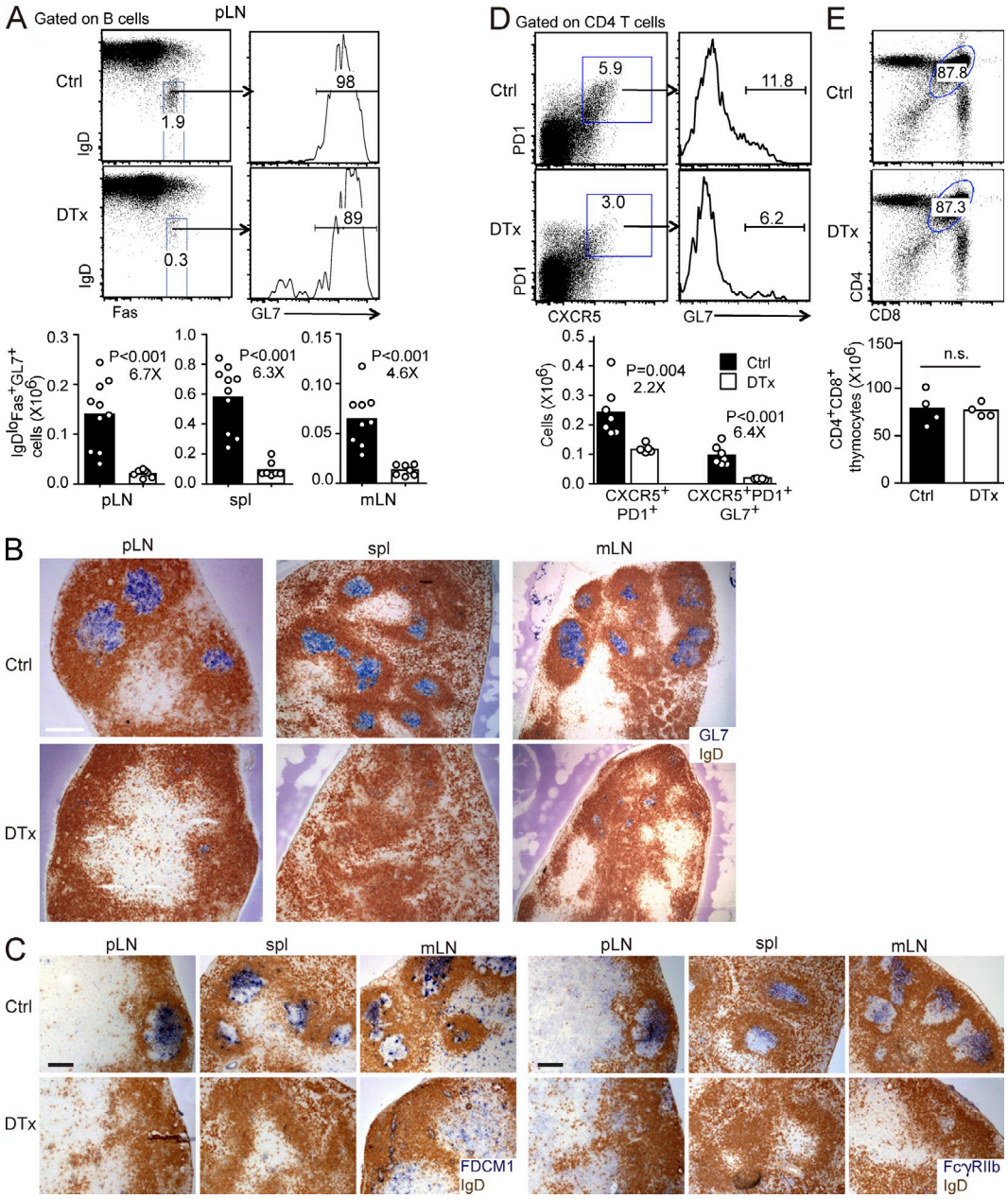

Figure 6. FDC ablation abrogates the GC response. CD21-DTR chimeras were immunized with SRBCs, control (Ctrl) or DTx treated at day 6, and analyzed at day 8. (A) Dot plots and histograms show flow cytometric analysis of GC B cells ($IgD^{low}Fas^+GL7^+$) in pLNs. Numbers show frequency of cells in indicated gate. Bar graphs show a summary of the data for $IgD^{low}Fas^+GL7^+$ GC B cell numbers in pLNs, spleen, and mLNs, in which bars represent means and dots represent individual mice. (B and C) Sections of pLNs, spleen, and mLNs stained to detect follicular B cells (IgD; brown) and GC B cells (GL7; blue; B) or GC FDCs (FDC-M1, left; and FcγRIIb, right; blue; C). Data are representative of at least three experiments (three mice per experiment). Bars: (B) 400 µm; (C) 200 µm. (D) Flow cytometric analysis of $CD4^+CXCR5^{hi}PD1^{hi}GL7^{hi}$ follicular helper T cells in pLNs. Bar graphs show cell numbers (bars represent means, and dots represent individual mice). (E) Frequency and number of CD4 and CD8 DP thymocytes in control- and DTx-treated mice at day 2 after treatment. In A, D, and E, statistical analysis was performed with the two-tailed unpaired Student's *t* test. Numbers below p-values in A and D indicate fold change. n.s., not significant.

loss of $CXCR5^{hi}PD1^+GL7^+$ GC-associated Tfh cells in the FDC-ablated mice (Fig. 6 D). Previous work has shown that GC B cells and double-positive (DP) thymocytes are sensitive to death induced by corticosteroids (Sentman et al., 1991; Secord et al., 1995). There was no effect of the DTx plus anti-DTx treatment on DP thymocyte numbers, making it unlikely that there had been an undetected surge in circulating corticosteroid levels (Fig. 6 E). These findings suggested that GC cells were dying rapidly after FDC ablation because of loss of local trophic support, although they did not exclude the possibility that the cells were traveling to other sites.

Published October 31, 2011

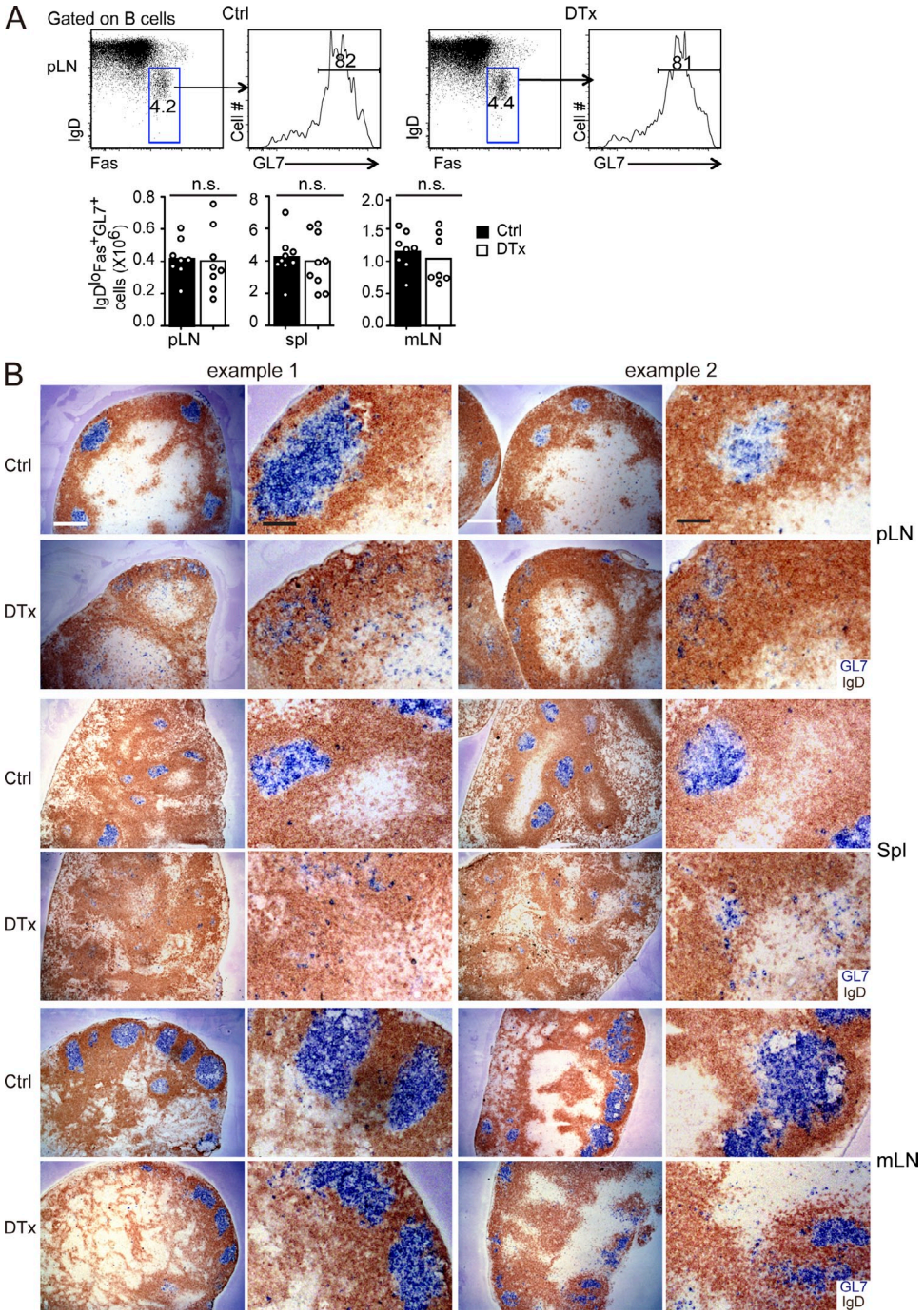

Figure 7. Splenic and pLN Bcl2 transgenic GC B cells are dispersed in the absence of FDCs. ROSA^{DTR+}CD21Cre^{+} mice that had been reconstituted with Bcl2 transgenic BM were immunized with SRBCs and then control (Ctrl) or DTx treated at day 6 and analyzed at day 8. (A) Flow cytometric analysis of GC B cells (IgD^{low}Fas^{+}GL7^{+}) in pLNs. Bar graphs show total cell numbers for pLNs, spleen (spl), and mLNs (bars indicate means, and dots represent individual mice). Statistical analysis was performed with the two-tailed unpaired Student's *t* test. n.s., not significant. (B) Sections of pLNs, spleen, and mLNs stained to detect GL7 (blue) and IgD (brown). Two examples of each type are shown at different magnifications. Data are representative of at least four experiments (more than six mice of each type). Bars: (white) 400 µm; (black) 100 µm.

FDCs are required for GC B cell clustering

In an effort to test whether rescuing GC B cell survival might allow GC clusters to persist in the absence of FDCs, CD21-DTR chimeric mice were generated using BM from B cell–specific Bcl2 transgenic mice (Strasser et al., 1990). The chimeras were then immunized to induce GC responses, treated with DTx, and analyzed 2 d later. Bcl2 overexpression fully rescued the GC B cell number that was detectable by flow cytometry in pLNs,

Published October 31, 2011

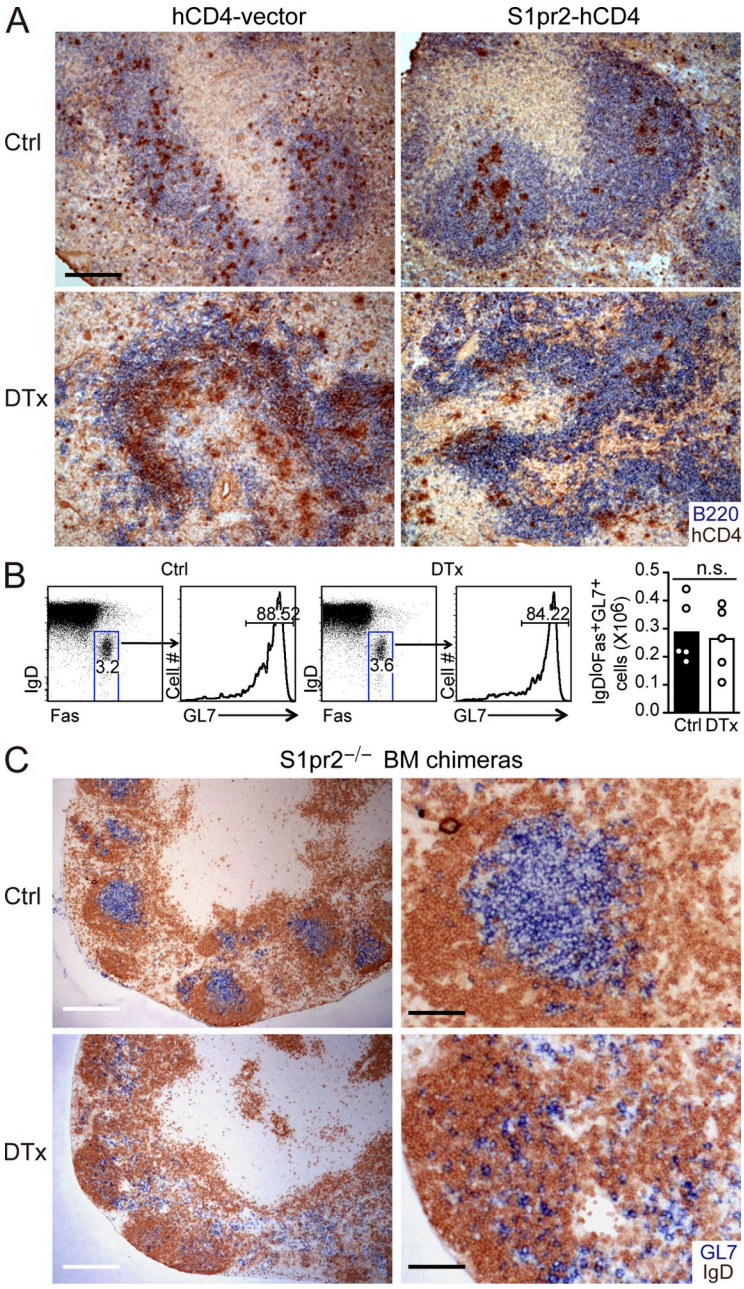

Figure 8. FDCs and S1PR2 cooperate to promote GC B cell clustering. (A) Distribution of B cells transduced with control (hCD4-vector) or S1PR2 encoding (S1pr2-hCD4) retroviral constructs 1 d after transfer to control (Ctrl)- or DTx-treated CD21-DTR chimera recipients. Splenic sections were stained to detect the transferred B cells (hCD4; brown) and endogenous B cells (B220; blue). Data are representative of three mice of each type analyzed in two experiments. (B and C) GC B cell location in mLNs of ROSA^{DTR+}CD21Cre^{+} mice reconstituted with *S1pr2*$^{-/-}$ BM, immunized 8 d before with SRBC and control or DTx treated 2 d before analysis. (B) Flow cytometric analysis and numbers of GC B cells (IgD^{low}Fas^{+}GL7^{+}) in mLNs. Statistical analysis was performed with the two-tailed unpaired Student's *t* test. n.s., not significant. (C) Sections of mLN stained for GL7 (blue) and IgD (brown). Bars: (A) 200 µm; (C, left) 400 µm; (C, right) 100 µm.

spleen, and mLNs of FDC-ablated mice (Fig. 7 A). Importantly, however, the rescued pLN and splenic GC B cells frequently failed to remain clustered in GCs and instead became dispersed within the B cell area and adjacent regions (Fig. 7 B). In mLNs, in contrast, GCs often persisted, although they sometimes appeared smaller and less organized (Fig. 7 B). These observations indicate that GC FDCs contribute to the clustering of GC B cells in spleen and pLNs but suggested that their role in this process may be redundant in mLNs.

S1PR2 cooperates with FDCs to mediate GC cell clustering

Recent work has established that the migration inhibitory sphingosine-1-phosphate (S1P) receptor, S1PR2, promotes confinement of GC B cells within GCs (Green et al., 2011). S1PR2 was suggested to promote cell clustering in response to a gradient of S1P that is at its lowest concentration within the center of the follicle, and consistent with the existence of this gradient, S1PR2 overexpression promotes B cell positioning at the follicle center (Green et al., 2011). Extracellular S1P has a half-life of only minutes (Skoura and Hla, 2009) and can be degraded by several cell membrane–associated enzymes (Spiegel and Milstien, 2003). B cells abundantly express these S1P degrading enzymes, and they efficiently degrade S1P (Green et al., 2011). To explore the possibility that S1P abundance was kept low in the follicle center because of FDC-mediated degradation, we transferred S1PR2-overexpressing B cells into FDC-ablated mice. S1pr2- but not vector-transduced cells continued to show a preference for positioning near the center of the B cell areas despite the absence of FDCs (Fig. 8 A). Perhaps as a consequence of the thinner and less organized nature of the FDC-ablated B cell areas, the clustered S1pr2-transduced cells were sometimes nearer the T zone than in wild-type controls (Fig. 8 A). We interpret these data as indicating that FDCs are not needed to maintain an S1P gradient, although by organizing B cells in follicles, they help shape the gradient. The evidence for the continued existence of an S1P gradient in the absence of FDCs led us to test the idea that FDCs and S1PR2 had redundant roles in clustering GC B cells in mLNs. S1PR2 deficiency has previously been shown to augment GC B cell survival because of reduced negative regulation of AKT (Green et al., 2011), leading us to consider the possibility that S1PR2-deficient GC B cells might survive after FDC ablation. Indeed, when CD21-DTR mice were generated that lacked hematopoietic S1PR2, DTx treatment no longer caused a loss of mLN GC B cells (Fig. 8 B). However, analysis of mLN tissue sections from these mice showed that the GL7^{+} GC areas had been disrupted and the GC B cells had become dispersed (Fig. 8 C). These findings suggest that FDCs and the

Published October 31, 2011

S1P–S1PR2 pathway work in an overlapping fashion to promote GC cell clustering. The data also support the conclusion that S1P concentrations in the B cell–rich areas most distant from vascular sinuses are kept S1P low by the degrading actions of B cells rather than FDCs. By causing larger and purer B cell clusters to form (i.e., follicles), FDCs likely help shape the S1P gradient, perhaps ensuring good alignment of the S1P low area with the region occupied by the FDCs.

DISCUSSION

We establish that FDCs help maintain primary follicle identity; in their absence, B cell areas rapidly lose homogeneity and overlap with areas containing T zone stromal cells as well as becoming infiltrated by DCs and T cells. An important aspect of follicle identity imparted by FDCs may be the establishment of a zone (the follicle) that limits access of phagocytes, cells which might otherwise cause rapid antigen clearance, helping make the follicle an antigen sanctuary that supports long-term antigen display (Cyster, 2010). Primary follicle FDCs also promote naive B cell migration, increasing the volume the cells survey for antigen in a given period of time. After GC formation, we show that FDCs promote the clustered state of GC B cells. The rapid death of many GC B cells after FDC ablation adds to other evidence suggesting that FDCs are needed, directly or indirectly, for maintenance of GC B cell viability.

Our detection of increased overlap between B cell–rich zones and ER-TR7, collagen type IV, and CCL21 expression in unimmunized spleen and LNs 2 d after FDC ablation might be explained in either of two ways. In the absence of FDCs, B cells may redistribute such that they become prevalent in areas that were previously T cell rich, such as interfollicular regions in LNs. Alternatively, FDCs may normally act, whether directly or indirectly (e.g., via B cells), to suppress T zone stromal features within B zones. Our current experiments do not allow us to fully distinguish between these possibilities, but we suspect that both processes are occurring. In spleen, the preponderance of B cells over T cells made an assessment of the FDC-lacking follicle-equivalent areas more compelling than was possible in LNs, and here there were clear instances of CCL21 expression extending into the B cell zones. The ER-TR7 and collagen type IV signals also appeared increased compared with the B cell areas of matched controls. During lymphoid tissue development, nascent B cell areas are occupied by ER-TR7$^+$ stromal cells and contain numerous collagen type IV–positive conduits; after B cells arrive, some stromal cells take on FDC features, and the T zone stromal network and collagen type IV fibers recede (Bajénoff and Germain, 2009). We suggest that the exclusion of T zone stromal cells from follicles may be promoted in part by FDCs. Because the follicular and T zone stromal cell networks are interconnected (McNagny et al., 1991; Yoshida et al., 1993; Ngo et al., 1999; Bajénoff and Germain, 2009), this suppressive cross talk may occur by direct intercellular communication. Alternatively, it might occur via FDC-induced modifications in the B cells.

Our findings of reduced total tissue CXCL13 transcript abundance in the spleen and mLNs after FDC ablation extends previous evidence that primary follicle FDCs are a source of this chemokine (Cyster et al., 2000; Allen and Cyster, 2008; Suzuki et al., 2010). The basis for the lack of effect of FDC ablation on CXCL13 transcript abundance in pLNs is not clear but might reflect a lesser contribution of FDCs to CXCL13 production in this tissue (Suzuki et al., 2010) or altered feedback controls leading to increased expression by non-FDC stromal cells.

The major source of BAFF for maintaining follicular B cell numbers was identified as a radiation-resistant, presumably stromal, cell type (Gorelik et al., 2003). Our finding that FDC ablation did not affect BAFF transcript abundance in unimmunized tissue adds to the previous finding of normal or elevated BAFF expression in LTβR-Fc–treated mice (Browning et al., 2005) and the presence of normal B cell numbers in LTα- and LTβR-deficient mice (Alimzhanov et al., 1997; Koni et al., 1997). It remains to be determined what radiation-resistant cell types are the predominant source of BAFF for naive B cells, although marginal reticular cells are candidates (Katakai et al., 2008). Our attempts to determine BAFF distribution in follicles using a commercial goat anti-BAFF reagent were unsuccessful as we observed similar staining patterns in lymphoid tissues from wild-type and BAFF-deficient (Gorelik et al., 2003) mice (not depicted). Therefore, we currently cannot exclude the possibility that BAFF is normally made by primary follicle FDCs and that there is compensatory up-regulation by other stromal cells after FDC ablation. As well as supporting naive B cell survival, BAFF has a role in maintenance of the GC response (Rahman et al., 2003; Vora et al., 2003). Our experiments have not addressed the contribution of FDCs to BAFF production in GCs.

GC FDCs have been suggested to be a source of B cell trophic factors (Victoratos et al., 2006; Allen and Cyster, 2008; Wu et al., 2009; Garin et al., 2010). Our data provide in vivo support for this function, although we do not exclude the possibility that the reduced viability of GC B cells after FDC ablation is secondary to the role of FDCs in keeping the cells clustered and thus in proximity to the antigen depot and follicular helper T cells. The expression of DTR in brain and kidney of CD21-DTR chimeric mice also means we cannot fully exclude the possibility that there were changes in other factors that adversely affected GC B cell survival. In addition to possibly being a source of BAFF, GC FDCs have been suggested to produce IL-6 (Wu et al., 2009), sonic hedgehog, and hepatocyte growth factor (Allen and Cyster, 2008), additional factors which might augment cell survival. Integrin-mediated adhesion to FDCs has also been suggested to contribute to GC B cell survival (Victoratos et al., 2006; Allen and Cyster, 2008; Garin et al., 2010). However, the impact of selective integrin ligand deficiency on FDCs in vivo has not yet been determined. The ability of S1PR2 deficiency to rescue mLN GC B cells from elimination after FDC ablation suggests that one trophic function of FDCs is to promote GC B cell clustering in the S1P-low area of the

Published October 31, 2011

follicle, minimizing S1PR2-mediated suppression of Akt prosurvival signaling (Green et al., 2011).

The mechanisms promoting GC B cell clustering to the follicle center and around the FDC network are beginning to be discerned (Cyster, 2010). CXCL13 is needed for B cells to accumulate in follicles and for GCs to form in their normal location (Ansel et al., 2000; Voigt et al., 2000; Allen et al., 2004). However, there is at this time no evidence that CXCL13 is more concentrated at the follicle center or within the GC than in other regions of the follicle, and CXCR5/CXCL13-deficient mice retain the ability to form GCs (Förster et al., 1996; Ansel et al., 2000). The similar disruption of primary follicle organization in CXCR5- and CXCL13-deficient mice and FDC-ablated mice might in part reflect the dependence of primary follicle FDCs on CXCL13-CXCR5–mediated induction of LTα1β2 in B cells (Förster et al., 1996; Ansel et al., 2000). EBI2 guides activated B cells to inter and outer follicular regions and down-regulation of EBI2 may be a necessary step in B cell movement to the follicle center. However, EBI2 deficiency does not prevent the normal formation of GCs (Pereira et al., 2009). Thus, we invoke the existence of an additional organizer made by GC FDCs that promotes clustering of GC B cells and follicular helper T cells.

Previous studies found that GC formation in mLNs was less lymphotoxin dependent than in other lymphoid tissues (Koni et al., 1997; Koni and Flavell, 1999), and our experiments extend these findings by showing that GC B cell clustering in mLNs is less FDC dependent than at other sites. However, FDCs do contribute to clustering in mLNs because combined removal of S1PR2 and FDCs caused dispersal of these cells. The basis for this different property of mLN GCs remains to be elucidated but may relate to distinct features of the mLN follicular stroma, to the presence of more robust S1P gradients in mLN follicles, and/or to influences of the chronic exposure to innate stimuli from the small intestine.

By demonstrating the critical role of FDCs in maintaining primary follicle identity and GC cell clustering, these results highlight the significance of FDC appearance at sites of chronic B cell accumulation such as in the inflamed synovium of rheumatoid arthritis patients. Our results suggest that therapeutic agents that selectively target FDC viability may potently disrupt GC B cell responses.

MATERIALS AND METHODS

Mice. C57BL/6J (B6), B6-Gt(ROSA)26Sortm1(HBEGF)Awai (Rosa-DTR), B6.Cg-Tg(BCL2)22Wehi/J (Eμ-Bcl2-22), and B6 CD45.1 mice were obtained from the Jackson Laboratory. B6.Tg(Cr2-Cre)3Cgn (CD21-Cre) mice were provided by K. Rajewsky (Immune Disease Institute, Boston, MA). To make BM chimera mice, lethally irradiated CD21-Cre × Rosa-DTR (CD21-DTR) mice were reconstituted for at least 6 wk with wild-type CD45.1, Bcl2 transgenic, or S1pr2$^{-/-}$ (Kono et al., 2004) BM as described previously (Pereira et al., 2009). For induction of spleen and pLN GCs, mice were immunized i.p. with 2 × 10^8 SRBCs (Colorado Serum Company) as described previously (Pereira et al., 2009) or s.c. at six sites across flanks. For imaging experiments, 10^7 CFSE-labeled B cells and 10^7 CMTMR-labeled T cells purified from B6 mice were injected i.v. into CD21-DTR chimeras to achieve a labeled cell frequency of 2–3% in LNs. Animals were housed in a specific pathogen–free environment in the Laboratory Animal Research Center at the University of California, San Francisco (UCSF), and all experiments conformed to ethical principles and guidelines approved by the UCSF Institutional Animal Care and Use Committee.

DTx treatment. For FDC ablation, mice were injected with DTx (in 10 mM Tris-HCl, pH 7.5, and 1 mM of EDTA buffer; EMD) either i.p. alone or with a split i.p. and at six s.c. doses across the flanks, to achieve a total of 1 ng/g body weight. In all experiments, except where stated for the initial experiments summarized in Fig. 1, mice were further treated 2.5–3 h later with an i.v. injection of DTx-specific goat polyclonal antibody (80 μg/mouse in PBS; Thermo Fisher Scientific).

Flow cytometry. Spleen and LN cells were isolated and stained as described previously (Pereira et al., 2009). For GC B cell staining, cells were stained with PE-conjugated anti-IgD (11-26c.2a; BD), PE-Cy7–conjugated anti-Fas (Jo2; BD), FITC-conjugated GL7 anti–T&B cell activation antigen or Ly-77 (BD), and PE-Cy5.5–conjugated anti-B220 (RA3-6B2; BD). For Tfh staining, cells were first stained with purified anti-CXCR5 (2G8; BD), then with biotin-conjugated anti–rat (Invitrogen), and lastly with streptavidin–Alexa Fluor 647, PE-conjugated anti-CD4 (RM4-5; BD), PE-Cy7–conjugated anti–PD-1 (RMP1-30; BioLegend), and FITC-GL7.

Immunohistochemistry, immunofluorescence, and in situ hybridization. Cryosections of 7 μm were fixed and stained immunohistochemically as previously described (Pereira et al., 2009) with the following first antibodies: PE-conjugated anti-IgD (11-26c.2a; BD), biotin-conjugated anti-CD35 (8C12; BD), rat anti–mouse fibroblast (ER-TR7; Novus Biologicals), rabbit anti–mouse Collagen IV (Abcam), rat anti–mouse B220 (RA-6B2; BD), biotin-conjugated anti–T/B cell activation antigen or Ly77 (GL7; BD), biotin conjugated anti–mouse CD3e (145-2C11; BD), goat anti–mouse CXCL13 (R&D Systems), goat anti–mouse CCL21 (R&D Systems), rat anti-CD169 (Ser4; P. Crocker, University of Glasgow, Glasgow, Scotland, UK), rat anti–mouse madcam-1 (MECA-367; BD), rat anti–mouse FDC (FDC-M1; BD), and FITC-conjugated rat anti–mouse CD16/32 (FcγRII/III; UCSF Hybridoma Core). For immunofluorescence, Alexa Fluor 647–conjugated anti-BP3, PE-conjugated anti-IgD, and FITC-conjugated anti-CD35 were used. In situ hybridization was performed as described previously (Ngo et al., 1999). In brief, sections were fixed in 4% paraformaldehyde, prehybridized for 3 h, and hybridized overnight at 58°C with digoxigenin-labeled probes. After washing at high stringency, sections were incubated with alkaline phosphatase–conjugated anti-digoxigenin antibody (Roche) and developed with NBT/BCIP (Roche). Images were all acquired with Axiovision version 4.8 using an Axio Observer Z1 microscope (Carl Zeiss).

Two-photon imaging. Explanted LNs were prepared for imaging as described previously (Suzuki et al., 2009; Green et al., 2011). Images were acquired with ZEN2009 (Carl Zeiss) using a 7MP two-photon microscope (Carl Zeiss) equipped with a Chameleon laser (Coherent). Each xy plane spans 616 μm × 616 μm at a resolution of 1.19 μm per pixel, and images of 39 xy planes with 3-μm z spacing (total depth of 114 μm) were formed every 30 s. Excitation wavelength was 870 nm. Emission filters were 440–480 nm for second harmonic, 500–550 nm for CFSE, and 570–640 nm for CMTMR. Videos were made and analyzed with Imaris 5.7.2 ×64 (Bitplane), and automated tracks were generated using a 6-μm spot size. Tracks were sorted based on duration, from longest to shortest, and the tracks were manually verified. Data from cells that could be tracked for at least 20 min were used for analysis (~50 from each experiment). The velocities, turning angles, and displacement of cells between each imaging frame were calculated with MATLAB (The MathWorks, Inc.). Annotation and final compilation of videos were performed with After Effects 7.0 software (Adobe). Video files were converted to MPEG format with AVI-MPEG Converter for Windows 1.5 (FlyDragon Software).

Retroviral transduction and cell transfer. Retroviral transductions with control (truncated NGFR) or S1pr2 retroviral constructs that also contained an IRES-truncated hCD4 reporter were performed with antigen and

CD40-activated EBI2$^{+/-}$ (Pereira et al., 2009) MD4 Ig transgenic B cells as described previously (Green et al., 2011). EBI2$^{+/-}$ B cells were used because CD40 activated B cells up-regulate EBI2, and this promotes their attraction to the outer follicle; by removing one copy of EBI2, the clustering influence of S1PR2 is more readily revealed (Green et al., 2011). Around 10^7 vector-transduced or 3×10^7 S1pr2-transduced cells were transferred and detected 1 d later using anti-hCD4 and a tyramide kit (TSA Biotin System; PerkinElmer).

Online supplemental material. Videos 1 and 2 show real-time imaging of B cell migration in control-treated pLNs. Videos 3 and 4 show real-time imaging of B cell migration in DTx-treated pLNs. Online supplemental material is available at http://www.jem.org/cgi/content/full/jem.20111449/DC1.

We thank Klaus Rajewsky for CD21-Cre mice and Chris Allen, Jeff Browning, and Tim Schmidt for comments on the manuscript.

This work was supported in part by National Institutes of Health grant AI45073. J.G. Cyster is an Investigator of the Howard Hughes Medical Institute.

The authors are not aware of any affiliations, memberships, funding, or financial holdings that might be perceived as affecting the objectivity of this study.

Submitted: 14 July 2011
Accepted: 6 October 2011

REFERENCES

Alimzhanov, M.B., D.V. Kuprash, M.H. Kosco-Vilbois, A. Luz, R.L. Turetskaya, A. Tarakhovsky, K. Rajewsky, S.A. Nedospasov, and K. Pfeffer. 1997. Abnormal development of secondary lymphoid tissues in lymphotoxin beta-deficient mice. *Proc. Natl. Acad. Sci. USA*. 94:9302–9307. http://dx.doi.org/10.1073/pnas.94.17.9302

Allen, C.D., and J.G. Cyster. 2008. Follicular dendritic cell networks of primary follicles and germinal centers: phenotype and function. *Semin. Immunol.* 20:14–25. http://dx.doi.org/10.1016/j.smim.2007.12.001

Allen, C.D., K.M. Ansel, C. Low, R. Lesley, H. Tamamura, N. Fujii, and J.G. Cyster. 2004. Germinal center dark and light zone organization is mediated by CXCR4 and CXCR5. *Nat. Immunol.* 5:943–952. http://dx.doi.org/10.1038/ni1100

Ansel, K.M., V.N. Ngo, P.L. Hyman, S.A. Luther, R. Förster, J.D. Sedgwick, J.L. Browning, M. Lipp, and J.G. Cyster. 2000. A chemokine-driven positive feedback loop organizes lymphoid follicles. *Nature*. 406:309–314. http://dx.doi.org/10.1038/35018581

Bajénoff, M., and R.N. Germain. 2009. B-cell follicle development remodels the conduit system and allows soluble antigen delivery to follicular dendritic cells. *Blood*. 114:4989–4997. http://dx.doi.org/10.1182/blood-2009-06-229567

Bajénoff, M., J.G. Egen, L.Y. Koo, J.P. Laugier, F. Brau, N. Glaichenhaus, and R.N. Germain. 2006. Stromal cell networks regulate lymphocyte entry, migration, and territoriality in lymph nodes. *Immunity*. 25:989–1001. http://dx.doi.org/10.1016/j.immuni.2006.10.011

Balogh, P., Y. Aydar, J.G. Tew, and A.K. Szakal. 2001. Ontogeny of the follicular dendritic cell phenotype and function in the postnatal murine spleen. *Cell. Immunol.* 214:45–53. http://dx.doi.org/10.1006/cimm.2001.1874

Browning, J.L. 2008. Inhibition of the lymphotoxin pathway as a therapy for autoimmune disease. *Immunol. Rev.* 223:202–220. http://dx.doi.org/10.1111/j.1600-065X.2008.00633.x

Browning, J.L., N. Allaire, A. Ngam-Ek, E. Notidis, J. Hunt, S. Perrin, and R.A. Fava. 2005. Lymphotoxin-beta receptor signaling is required for the homeostatic control of HEV differentiation and function. *Immunity*. 23:539–550. http://dx.doi.org/10.1016/j.immuni.2005.10.002

Cupedo, T., F.E. Lund, V.N. Ngo, T.D. Randall, W. Jansen, M.J. Greuter, R. de Waal-Malefyt, G. Kraal, J.G. Cyster, and R.E. Mebius. 2004. Initiation of cellular organization in lymph nodes is regulated by non-B cell-derived signals and is not dependent on CXC chemokine ligand 13. *J. Immunol.* 173:4889–4896.

Cyster, J.G. 2010. B cell follicles and antigen encounters of the third kind. *Nat. Immunol.* 11:989–996. http://dx.doi.org/10.1038/ni.1946

Cyster, J.G., K.M. Ansel, K. Reif, E.H. Ekland, P.L. Hyman, H.L. Tang, S.A. Luther, and V.N. Ngo. 2000. Follicular stromal cells and lymphocyte homing to follicles. *Immunol. Rev.* 176:181–193. http://dx.doi.org/10.1034/j.1600-065X.2000.00618.x

El Shikh, M.E., R.M. El Sayed, S. Sukumar, A.K. Szakal, and J.G. Tew. 2010. Activation of B cells by antigens on follicular dendritic cells. *Trends Immunol.* 31:205–211. http://dx.doi.org/10.1016/j.it.2010.03.002

Förster, R., A.E. Mattis, E. Kremmer, E. Wolf, G. Brem, and M. Lipp. 1996. A putative chemokine receptor, BLR1, directs B cell migration to defined lymphoid organs and specific anatomic compartments of the spleen. *Cell*. 87:1037–1047. http://dx.doi.org/10.1016/S0092-8674(00)81798-5

Fu, Y.-X., and D.D. Chaplin. 1999. Development and maturation of secondary lymphoid tissues. *Annu. Rev. Immunol.* 17:399–433. http://dx.doi.org/10.1146/annurev.immunol.17.1.399

Garin, A., M. Meyer-Hermann, M. Contie, M.T. Figge, V. Buatois, M. Gunzer, K.M. Toellner, G. Elson, and M.H. Kosco-Vilbois. 2010. Toll-like receptor 4 signaling by follicular dendritic cells is pivotal for germinal center onset and affinity maturation. *Immunity*. 33:84–95. http://dx.doi.org/10.1016/j.immuni.2010.07.005

Gorelik, L., K. Gilbride, M. Dobles, S.L. Kalled, D. Zandman, and M.L. Scott. 2003. Normal B cell homeostasis requires B cell activation factor production by radiation-resistant cells. *J. Exp. Med.* 198:937–945. http://dx.doi.org/10.1084/jem.20030789

Green, J.A., K. Suzuki, B. Cho, L.D. Willison, D. Palmer, C.D. Allen, T.H. Schmidt, Y. Xu, R.L. Proia, S.R. Coughlin, and J.G. Cyster. 2011. The sphingosine 1-phosphate receptor $S1P_2$ maintains the homeostasis of germinal center B cells and promotes niche confinement. *Nat. Immunol.* 12:672–680. http://dx.doi.org/10.1038/ni.2047

Hase, H., Y. Kanno, M. Kojima, K. Hasegawa, D. Sakurai, H. Kojima, N. Tsuchiya, K. Tokunaga, N. Masawa, M. Azuma, et al. 2004. BAFF/BLyS can potentiate B-cell selection with the B-cell coreceptor complex. *Blood*. 103:2257–2265. http://dx.doi.org/10.1182/blood-2003-08-2694

Kabashima, K., T.A. Banks, K.M. Ansel, T.T. Lu, C.F. Ware, and J.G. Cyster. 2005. Intrinsic lymphotoxin-beta receptor requirement for homeostasis of lymphoid tissue dendritic cells. *Immunity*. 22:439–450. http://dx.doi.org/10.1016/j.immuni.2005.02.007

Katakai, T., H. Suto, M. Sugai, H. Gonda, A. Togawa, S. Suematsu, Y. Ebisuno, K. Katagiri, T. Kinashi, and A. Shimizu. 2008. Organizer-like reticular stromal cell layer common to adult secondary lymphoid organs. *J. Immunol.* 181:6189–6200.

Koni, P.A., and R.A. Flavell. 1999. Lymph node germinal centers form in the absence of follicular dendritic cell networks. *J. Exp. Med.* 189:855–864. http://dx.doi.org/10.1084/jem.189.5.855

Koni, P.A., R. Sacca, P. Lawton, J.L. Browning, N.H. Ruddle, and R.A. Flavell. 1997. Distinct roles in lymphoid organogenesis for lymphotoxins alpha and beta revealed in lymphotoxin beta-deficient mice. *Immunity*. 6:491–500. http://dx.doi.org/10.1016/S1074-7613(00)80292-7

Kono, M., Y. Mi, Y. Liu, T. Sasaki, M.L. Allende, Y.P. Wu, T. Yamashita, and R.L. Proia. 2004. The sphingosine-1-phosphate receptors S1P1, S1P2, and S1P3 function coordinately during embryonic angiogenesis. *J. Biol. Chem.* 279:29367–29373. http://dx.doi.org/10.1074/jbc.M403937200

Kranich, J., N.J. Krautler, E. Heinen, M. Polymenidou, C. Bridel, A. Schildknecht, C. Huber, M.H. Kosco-Vilbois, R. Zinkernagel, G. Miele, and A. Aguzzi. 2008. Follicular dendritic cells control engulfment of apoptotic bodies by secreting Mfge8. *J. Exp. Med.* 205:1293–1302. http://dx.doi.org/10.1084/jem.20071019

Lu, T.T., and J.G. Cyster. 2002. Integrin-mediated long-term B cell retention in the splenic marginal zone. *Science*. 297:409–412. http://dx.doi.org/10.1126/science.1071632

Martin, F., and J.F. Kearney. 2002. Marginal-zone B cells. *Nat. Rev. Immunol.* 2:323–335. http://dx.doi.org/10.1038/nri799

McNagny, K.M., R.P. Bucy, and M.D. Cooper. 1991. Reticular cells in peripheral lymphoid tissues express the phosphatidylinositol-linked BP-3 antigen. *Eur. J. Immunol.* 21:509–515. http://dx.doi.org/10.1002/eji.1830210238

Ngo, V.N., H. Korner, M.D. Gunn, K.N. Schmidt, D.S. Riminton, M.D. Cooper, J.L. Browning, J.D. Sedgwick, and J.G. Cyster. 1999. Lymphotoxin α/β and tumor necrosis factor are required for stromal

cell expression of homing chemokines in B and T cell areas of the spleen. *J. Exp. Med.* 189:403–412. http://dx.doi.org/10.1084/jem.189.2.403

Pereira, J.P., L.M. Kelly, Y. Xu, and J.G. Cyster. 2009. EBI2 mediates B cell segregation between the outer and centre follicle. *Nature.* 460:1122–1126.

Phan, T.G., J.A. Green, E.E. Gray, Y. Xu, and J.G. Cyster. 2009. Immune complex relay by subcapsular sinus macrophages and noncognate B cells drives antibody affinity maturation. *Nat. Immunol.* 10:786–793. http://dx.doi.org/10.1038/ni.1745

Rahman, Z.S., S.P. Rao, S.L. Kalled, and T. Manser. 2003. Normal induction but attenuated progression of germinal center responses in BAFF and BAFF-R signaling–deficient mice. *J. Exp. Med.* 198:1157–1169. http://dx.doi.org/10.1084/jem.20030495

Roozendaal, R., and M.C. Carroll. 2007. Complement receptors CD21 and CD35 in humoral immunity. *Immunol. Rev.* 219:157–166. http://dx.doi.org/10.1111/j.1600-065X.2007.00556.x

Schmidt-Supprian, M., and K. Rajewsky. 2007. Vagaries of conditional gene targeting. *Nat. Immunol.* 8:665–668. http://dx.doi.org/10.1038/ni0707-665

Secord, E.A., J.M. Edington, and G.J. Thorbecke. 1995. The Emu-bcl-2 transgene enhances antigen-induced germinal center formation in both BALB/c and SJL mice but causes age-dependent germinal center hyperplasia only in the lymphoma-prone SJL strain. *Am. J. Pathol.* 147:422–433.

Sentman, C.L., J.R. Shutter, D. Hockenbery, O. Kanagawa, and S.J. Korsmeyer. 1991. bcl-2 inhibits multiple forms of apoptosis but not negative selection in thymocytes. *Cell.* 67:879–888. http://dx.doi.org/10.1016/0092-8674(91)90361-2

Skoura, A., and T. Hla. 2009. Regulation of vascular physiology and pathology by the S1P2 receptor subtype. *Cardiovasc. Res.* 82:221–228. http://dx.doi.org/10.1093/cvr/cvp088

Spiegel, S., and S. Milstien. 2003. Sphingosine-1-phosphate: an enigmatic signalling lipid. *Nat. Rev. Mol. Cell Biol.* 4:397–407. http://dx.doi.org/10.1038/nrm1103

Strasser, A., A.W. Harris, D.L. Vaux, E. Webb, M.L. Bath, J.M. Adams, and S. Cory. 1990. Abnormalities of the immune system induced by dysregulated bcl-2 expression in transgenic mice. *Curr. Top. Microbiol. Immunol.* 166:175–181.

Suzuki, K., I. Grigorova, T.G. Phan, L.M. Kelly, and J.G. Cyster. 2009. Visualizing B cell capture of cognate antigen from follicular dendritic cells. *J. Exp. Med.* 206:1485–1493. http://dx.doi.org/10.1084/jem.20090209

Suzuki, K., M. Maruya, S. Kawamoto, K. Sitnik, H. Kitamura, W.W. Agace, and S. Fagarasan. 2010. The sensing of environmental stimuli by follicular dendritic cells promotes immunoglobulin A generation in the gut. *Immunity.* 33:71–83. http://dx.doi.org/10.1016/j.immuni.2010.07.003

Szakal, A.K., M.H. Kosco, and J.G. Tew. 1989. Microanatomy of lymphoid tissue during humoral immune responses: structure function relationships. *Annu. Rev. Immunol.* 7:91–109. http://dx.doi.org/10.1146/annurev.iy.07.040189.000515

Tew, J.G., G.F. Burton, L.I. Kupp, and A. Szakal. 1993. Follicular dendritic cells in germinal center reactions. *Adv. Exp. Med. Biol.* 329:461–465. http://dx.doi.org/10.1007/978-1-4615-2930-9_77

Victoratos, P., J. Lagnel, S. Tzima, M.B. Alimzhanov, K. Rajewsky, M. Pasparakis, and G. Kollias. 2006. FDC-specific functions of p55TNFR and IKK2 in the development of FDC networks and of antibody responses. *Immunity.* 24:65–77. http://dx.doi.org/10.1016/j.immuni.2005.11.013

Voigt, I., S.A. Camacho, B.A. de Boer, M. Lipp, R. Förster, and C. Berek. 2000. CXCR5-deficient mice develop functional germinal centers in the splenic T cell zone. *Eur. J. Immunol.* 30:560–567. http://dx.doi.org/10.1002/1521-4141(200002)30:2<560::AID-IMMU560>3.0.CO;2-T

Vora, K.A., L.C. Wang, S.P. Rao, Z.Y. Liu, G.R. Majeau, A.H. Cutler, P.S. Hochman, M.L. Scott, and S.L. Kalled. 2003. Cutting edge: germinal centers formed in the absence of B cell-activating factor belonging to the TNF family exhibit impaired maturation and function. *J. Immunol.* 171:547–551.

Wang, Y.G., K.D. Kim, J. Wang, P. Yu, and Y.X. Fu. 2005. Stimulating lymphotoxin beta receptor on the dendritic cells is critical for their homeostasis and expansion. *J. Immunol.* 175:6997–7002.

Wu, Y., M.E. El Shikh, R.M. El Sayed, A.M. Best, A.K. Szakal, and J.G. Tew. 2009. IL-6 produced by immune complex-activated follicular dendritic cells promotes germinal center reactions, IgG responses and somatic hypermutation. *Int. Immunol.* 21:745–756. http://dx.doi.org/10.1093/intimm/dxp041

Yoshida, K., N. Matsuura, N. Tamahashi, and T. Takahashi. 1993. Development of antigenic heterogeneity in the splenic meshwork of severe combined immunodeficient (SCID) mice after reconstitution with T and B lymphocytes. *Cell Tissue Res.* 272:1–10. http://dx.doi.org/10.1007/BF00323564

SUPPLEMENTAL MATERIAL

Wang et al., http://www.jem.org/cgi/content/full/jem.20111449/DC1

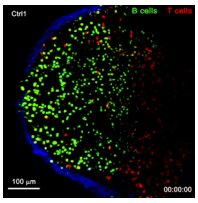

Video 1. Real-time imaging of B cell migration in a control-treated pLN (example 1). This video is a 30-min time-lapse sequence of 21-µm z-projection images. Time is shown in hours/minutes/seconds.

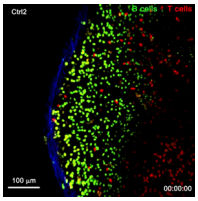

Video 2. Real-time imaging of B cell migration in a control-treated pLN (example 2). This video is a 30-min time-lapse sequence of 21-µm z-projection images. Time is shown in hours/minutes/seconds.

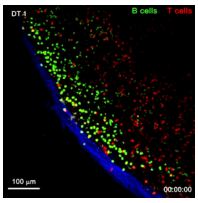

Video 3. Real-time imaging of B cell migration in a DTx-treated pLN (example 1). This video is a 30-min time-lapse sequence of 21-µm z-projection images. Time is shown in hours/minutes/seconds.

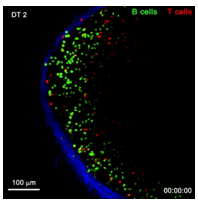

Video 4. Real-time imaging of B cell migration in a DTx-treated pLN (example 2). This video is a 30-min time-lapse sequence of 21-µm z-projection images. Time is shown in hours/minutes/seconds.